Case Studies in Thermal Engineering 49 (2023) 103256

Contents lists available at ScienceDirect

Case Studies in Thermal Engineering

journal homepage: www.elsevier.com/locate/csite

Pulsating heat pipe and embedded heat pipe heat spreaders for modular electronics cooling

Sai Kiran Hota [*], Kuan-Lin Lee [**], Brett Leitherer, George Elias, Greg Hoeschele, Srujan Rokkam [***]

Advanced Cooling Technologies, Inc., 1046 New Holland Ave., Lancaster, PA, 17601, USA

ARTICLE INFO

Handling Editor: Dr Y Su

Keywords:
Pulsating heat pipe (PHP)
EHP
Two-phase fluid
Heat spreader
Electronics cooling
Thermal management

ABSTRACT

Two-phase-based heat spreaders are highly sought electronics cooling solutions due to their superior thermal performance over conventional conduction plates. Along with good thermal performance, Pulsating Heat Pipes (PHPs) potentially have thickness, shape matching and cost benefits over Embedded Heat Pipe (EHP) heat spreader solutions. In this manuscript, the thermal performance of PHP charged with three different fluids-propylene, R245fa, and acetone was experimentally determined for different sink temperatures and compared to an EHP heat spreader. A mathematical model to predict the thermal performance of the PHP was developed and validated against experimental results. It was determined that at low sink temperatures, PHP charged with propylene performs better than or similar to an EHP heat spreader with up to 7.8 times higher effective thermal conductivity over a conduction plate. However, at moderate temperatures above >40 °C, propylene PHP dries out faster than the EHP plate. PHP performance with R245fa and acetone improves with increasing heater power. Effective thermal conductivity improved by 2.5 times with R245fa PHP and by 4 times with acetone PHP over the conventional plate but was lower than the EHP plate whose effective thermal conductivity was 17.3 times higher. However, weight comparison showed PHP to be lighter than the EHPs.

Nomenclature

Symbols

A	Cross-sectional area, m^2
C_p	Specific heat capacity, J/kg-K
d	Channel hydraulic diameter, mm/m
f	Friction factor
g	Acceleration due to gravity, 9.81 m^2/s
h	Heat transfer coefficient, W/m^2-K
h_{fg}	Enthalpy of vaporization, J/kg
k	Thermal conductivity, W/m-K

* Corresponding author.
** Corresponding author.
*** Corresponding author.
E-mail addresses: saikiran.hota@1-act.com (S.K. Hota), kuan-lin.lee@1-act.com (K.-L. Lee), srujan.rokkam@1-act.com (S. Rokkam).

https://doi.org/10.1016/j.csite.2023.103256
Received 1 April 2023; Received in revised form 20 June 2023; Accepted 2 July 2023
Available online 5 July 2023

L	Length, M
m	Mass of fluid, kg
P	Pressure, Pa
Q	Heat rate, W
R	Thermal resistance, °C/W
r_b	Bend radius m
T	Temperature, °C
u	Velocity, m/s
x	Vapor quality

Greek symbols

σ	Surface tension, N/m
μ	Viscosity, Pa.s
ρ	Density, Kg/m^3

Subscripts

cond	Condenser
cr	Critical
evap	Evaporator
l	Liquid
v	Vapor
w	Wall

Acronyms

EHP	Embedded heat pipe
PHP	Pulsating heat pipe
LN2	Liquid nitrogen

1. Introduction

Miniaturization of high-density power electronics requires advanced thermal management solutions that can handle high heat fluxes [1]. Various forms of efficient electronics cooling solutions such as spray cooling, radiative cooling, minichannel heat sinks, heat pipes heat spreaders, phase change material-based heat sinks, etc. have been developed [2]. Heat pipes have been developed commercially due to their good size, weight, and thermal performance attributes. Heat pipes also operate passively, so they don't need to pump fluid for heat extraction from electronics.

Heat pipes can be embedded into the base plate, otherwise referred to as Embedded Heat Pipe (EHP), for planar heat spreading capabilities. The thermal conductivities of EHPs are several times higher than conduction plates [3]. The heat transfer in a heat pipe is by vaporization of the working fluid at the evaporator and simultaneous returning condensed liquid from the condenser through the wick structure. Weyant et al. [4], fabricated and tested EHP heat spreaders in an AlSiC base plate. They embedded copper-water heat pipes into the aluminum rich side using two types of wick structures. At a heater power of 150 W (heat flux 37.5 W/cm^2), the maximum temperature on the EHP was 84 °C (wick type #1) and 75 °C for (wick type #2). In comparison, the maximum temperature on AlSiC only plate was 124 °C. While the thermal conductivity of AlSiC plate alone was 200 W/m-K, they noted that the EHP improved the plate thermal conductivity to 417–492 W/m-K, depending on the wick type. Zhu et al. [5], studied energy saving potential of EHP based heat sinks against standard copper heat sink in the context of data centers. They fabricated and tested three types of heat sinks: EHP heat sink in aluminum with U-shaped heat pipes (type A), planar heat pipe-based copper heat sink (type B), and solid copper plate based heat sink (type C). These heat sinks were placed in a wind tunnel and tested with air-flowing through them. They noted that the thermal resistance of the of the type B heat sink was slightly lower than type A heat sink, but almost comparable when measured against conventional type C heat sink. As such, this reduction in thermal resistance reduced maximum temperature, thereby, estimating power savings up to 13% with type B heat sink and up to 18% with type A heat sink. In another published literature, Salem et al. [6], compared cooling performance of a EHP embedded PCB using aluminum and polymer base plates. About 50% reduction in thermal resistance was noted with PCB-EHP in comparison to the conventional heat dissipation option. Another study by Muneeshwaran et al. [7], compared the performance of air-cooled standard fin-heat sink connected to a flat plate heat spreader and a vapor-chamber based spreader with EHPs (VC + HP). The heat sink plate dimensions was 180 mm x 120 mm x 29 mm. In the VC + HP type sink, U-shaped heat pipes of diameter 6 mm and sintered copper wicks of average size 150 μm was used. At a heat load of 500 W, the maximum chip temperature on the conventional heat sink was over 110 °C, while the improved heat sink had maximum temperature up to 50 °C lower. In general, literature shows that EHP based heat spreaders (or sinks) significantly improve the heat dissipation performance in an electronics system. While, the performance of EHPs for terrestrial applications is noted, Ababneh et al.

[8], successfully demonstrated superior thermal spreading performance of the EHP heat spreaders on the International Space Station. In general, the heat pipe technology is well established and proven for good heat spreading compared to conventional conduction plates. Several types of commercial Embedded Heat Pipe (EHP) heat spreaders: e.g., Hi-K™ plate [1], Isobar® heat pipes [2], etc. are available.

Another form of heat pipe called Pulsating Heat Pipe (PHP) has also been attracting significant interest over the years. PHPs typically have end-to-end connected meandering tubes with small channel diameters. Smaller channels result in the distribution of the working fluid into liquid slugs and vapor plugs due to capillary forces. The heat transfer in a PHP is through pulsation of continuously expanding and contracting vapor plugs due to simultaneous heat addition (in the evaporator) and heat removal (in the condenser) leading to evaporation and condensation of the working fluid [9,10]. The heat transfer performance of PHP can be similar to that of heat pipes with effective thermal conductivity reaching up to 1000 W/m-K and higher [11,12]. Several tests with integrated PHP heat spreaders have been performed and reported in the literature. Hoesing and Michna [13] integrated a 20 turn flat plate PHP into an aluminum plate of dimensions 177 mm x 127 mm x 3.75 mm. The cross-section of the channels was 2 mm x 2 mm. Water was used as the working fluid. At 90° inclination angle, they achieved thermal resistance of 0.5 °C/W. In comparison, the thermal resistance of the conventional heat spreader (empty PHP) was 1.97 °C/W. In another study by Luan et al. [14], radial PHP with tesla valves were tested. Heat was applied on the center of the PHP over a 30 mm x 30 mm area. Cold water block was attached on the other side of the PHP and so, the rest of the area was used as the condenser. When a copper spacer was incorporated between the PHP and the cold water block, the average plate temperature difference was up to 88 °C with conventional copper slab, while with the PHP, the temperature difference was just below 60 °C, showing up to 46% improvement in heat spreading. In another publication, Qu and Yang [15] investigated performance of a circular and square channels PHPs embedded in an aluminum plate of size 250 mm x 60 mm x 4 mm. They noted that the effective thermal conductivity could reach up to 3200 W/m-K, while that of empty PHP was only 245.5 W/m-K. The above-mentioned PHPs were usually diffusion bonded. The performance of the PHPs fabricated by additive manufacturing were also noted in literature. Thompson et al. [16], additively manufactured a PHP with Ti–6Al–4V using Selective Laser Melting technique and particle size typically below 45 μm. The diameter of the channels was 1.53 mm. The dimensions of the PHP plate was 50.8 mm x 38.1 mm x 15.75 mm. The effective thermal conductivity of the empty Ti–6Al–4V PHP was 18 W/m-K. In contrast, when the PHP was charged with DI water, effective thermal conductivity up to 110 W/m-K was obtained at power levels. Under stable operating conditions, the performance of the PHP was almost similar in horizontal and vertical orientation. In another study, Tian et al. [17], fabricated a ceramic PHP heat spreader of size 37.2 mm x 61.7 mm x 4.6 mm with alumina using additive manufacturing. Using water as the working fluid, they observed thermal resistance of the PHP heat spreader was 97% lower than the plain alumina plate. PHPs can be lighter than the heat pipe heat spreaders as the capillary channels can be engraved within the base plate and the removed solid material is replaced partly with relatively low-density working fluid. Also, PHP offers shape-matching capabilities like accommodating sharp corners which is difficult to realize with heat pipes mostly due to rigid envelope [10,18].

However, PHPs are still in developmental stages with significant efforts dedicated to understanding the operating behavior, heat transport limitations, the influence of geometry, working fluids, operating conditions, etc. PHP requires superheat for start-up and operation. The startup heat depends on the degree of superheat required for the working fluid [19–21]. After start-up, the performance of the PHP generally improves with increasing heater power until dry-out. In general, it is noted that working fluids with high $\frac{\partial P}{\partial T}|_{sat}$ delivers high performance. Additionally, other thermo-physical properties like liquid density, latent heat of vaporization, etc. must be considered during working fluid selection [22]. The optimal fluid charge depends on several factors, but it is agreed that 20–80% must be present for efficient operation [23]. PHP geometrical parameters like channel hydraulic diameter, evaporator/condenser length, etc. affect PHP performance [23]. Within the critical diameter limit, a larger hydraulic diameter improves PHP performance but results in faster dry-out. Likewise, a larger condenser is favorable as the probability of liquid formation near the evaporator increases. Several experimental and numerical works characterizing PHP performance in comparison to conventional conduction-only devices have been published over the years. However, PHP's will compete with state-of-the art technologies like EHP. This manuscript provides discussion on performance improvement and comparison of PHP and EHP heat spreaders against conventional conduction only plate. More specifically, on the experimental side, PHP was charged with multiple working fluids – propylene, acetone, and R245fa and compared against a EHP heat spreader (copper-water heat pipes embedded into an aluminum plate) to identify suitable PHP working fluid and ideal operating temperature for the heat spreaders. Additionally, an analytical model based on the spring-mass-damper approach was developed to predict PHP thermal performance [24–26]. This mathematical approach developed can be used to develop a PHP with a performance similar to or better than that of EHP. The thermal performance improvement and tentative weight of the heat spreaders was noted against a conduction only heat spreader.

2. Methodology

In this manuscript, the performance of PHP and EHP heat spreaders for electronics cooling are determined and compared experimentally. Quasi-steady state testing method was adopted to determine the heat spreader performance. The sink was maintained at a constant temperature and the heater power was varied after recording steady-state wall temperatures of the heat spreader. An analytical model for PHP performance prediction was developed and validated against experimental data presented here and from other literature. The schematic of the heat spreaders and the experimental setup are shown in Fig. 1.

[1] https://www.1-act.com/products/hik-plates/.
[2] https://www.acrolab.com/development-of-thermal-solution-for-card-chassis-with-embedded-isobar-heat-pipes/.

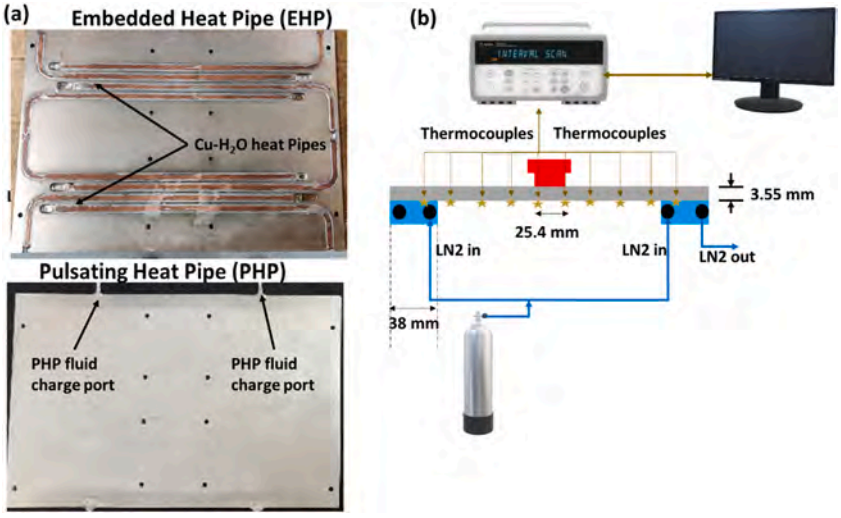

Fig. 1. (a) Flat plate EHP and PHP heat spreaders; (b) Schematic of the experimental test system for comparative heat spreader performance characterization.

2.1. PHP and EHP heat spreaders

Both PHP and EHP heat spreaders of size 230 mm x 160 mm x 3.55 mm (~6 U card dimensions [27]) were fabricated and tested to compare their performance. The PHP was fabricated by vacuum brazing of engraved aluminum plates. The PHP heat spreader consisted of two separate identical working fluid channels of size 1.6 mm with provision for charging the working fluids separately. The EHP heat spreader had 8 copper-water heat pipes embedded in an aluminum base plate. Holes were provided at the center and at the edges of the heat spreader to secure the heater blocks (evaporator) and cold plates (condensers).

2.2. Experimental setup and procedure

In general, the heat spreaders interface with the electronics chips on one side and reject heat from the other side or from the edges through card retainers in enclosed in a chassis or heat sink attachment [27,28]. The electronics chips are the sources of heat which is dissipated over a large area by these heat spreaders. The heat spreaders then reject heat to the downstream interfacing thermal links or the heat sink. To simulate heat source, two heater blocks of size 25 mm x 25 mm were attached at the center of the heat spreaders to supply desired heat input. Two cartridge heaters were inserted into the heater blocks for heat input. The heating was controlled by an external DC source attached to a power meter. To reduce thermal contact resistance between the chips-spreaders, spreaders-heat sink, thermal interface materials are used during the packaging [28]. Here, a layer of silicone thermal paste was used as the thermal interface between the heater block and the heat spreader to reduce the thermal contact resistance. For heat rejection. two cold plates, each 38 mm wide were attached to the edges of the heat spreaders. A grafoil sheet was placed between the heat spreader and the cold plate to reduce the thermal contact resistance. The sink was maintained at a constant temperature by flowing liquid nitrogen (LN2) through the cold plate tubes. The LN2 flow rate was controlled by a feedback control that monitors the sink temperature. Thermocouples of type-T were attached to the heat spreaders to measure and record the temperature via the Keithley data acquisition.

2.3. Data reduction and uncertainty analysis

The thermal performance of the heat spreaders can be calculated as:

$$R = \frac{\Delta T}{Q} \qquad \text{(eq. 1)}$$

Where, ΔT is the temperature difference betn the average evaporator and the average condenser wall temperatures, and Q is the heater power. From the above equation, the thermal conductivity of the PHP can be calculated as [23]:

$$k = \frac{QL}{A\Delta T} = \frac{L}{AR} \qquad \text{(eq. 2)}$$

Where L is the distance between the PHP evaporator and the condenser and A is the plate cross-section area.

The uncertainty in experimental measurement can be calculated as:

$$U = \sqrt{\left(\frac{\delta Q}{Q}\right)^2 + \left(\frac{\delta T_c}{\Delta T}\right)^2 + \left(\frac{\delta T_e}{\Delta T}\right)^2} \qquad \text{(eq. 3)}$$

The measured accuracy of the heater power was ±2.5 W and the thermocouple accuracy was ±0.1 °C. The Maximum uncertainty calculated by eq. (3) was 5.05%. Considering a nominal heat loss coefficient of 2 W/m^2-K through the insulation, the estimated

maximum heat loss at 500 W heater power was ~2.25%.

2.4. PHP working fluids

The PHP working fluids must satisfy the critical diameter condition which is given by the Bond number limit as:

$$d_{crit} = 2\sqrt{\frac{\sigma}{(\rho_l - \rho_v)g}} \quad \text{(eq. 4)}$$

Eq. (4) corresponds to a maximum Bond number limit of 4, which is commonly used. Three working fluids: propylene, acetone, and R245fa were selected for PHP performance testing.

For the chosen 1.6 mm channel size, as shown in Fig. 2, the maximum PHP operating temperature for propylene and R245fa charged PHP can potentially operate up to 70 °C, which is 5 °C below the electronics failure temperature [2]. Acetone has a higher critical diameter for the operating temperature range. The working fluid charge in the PHP during the test was 50%.

2.5. Analytical model for PHP performance prediction

An analytical thermal resistance model, as shown in the schematic in Fig. 3 (a), was developed for PHP performance prediction. The analytical model is based on the spring-mass-damper approach [24,25] to solve the second-order differential equation to determine the oscillation and thereby the PHP performance. The solution scheme for PHP performance prediction is shown in Fig. 3 (b). The PHP geometry and thermo-physical properties of the working fluid and the operating boundary conditions-heater power and condenser wall temperatures are specified. Then the equations are solved by the solution scheme as follows: An initial guess velocity is provided to solve for the temperature drop. This is then used to solve the second order-differential equations to yield a new velocity. This procedure iterates until the solution converges to a residual tolerance of 10^{-6}. The overall temperature drop, and thus, the PHP thermal performance can be determined.

To solve the performance prediction model, representative flow boiling equations for fluid evaporation proposed by Chen [29] and the two-phase condensation model proposed by Shah [30] were used.

2.5.1. Evaporator heat transfer

The heat added to the PHP evaporator wall is conducted through the wall. The heat is then transferred to the working fluid which vaporizes. The corresponding heat transfer coefficient of the working fluid can be given as [29,31]:

$$h_{evap} = h_{mic} + h_{mac} \quad \text{(eq. 5)}$$

Where h_{mic} is the heat transfer coefficient associated with microscopic fluid latent heat change and h_{mac} is the heat transfer associated with the macroscopic convective flow of the bulk fluid. The heat transfer associated with phase change is given as [29]:

$$h_{mic} = 0.00122\left(\frac{k_l^{0.79} C_{pl}^{0.45} \rho_l^{0.49}}{\sigma^{0.5} \mu_l^{0.29} h_{fg}^{0.24} \rho_v^{0.24}}\right)(T_w - T_{sat}(P_l))^{0.24}(P_w - P_l)^{0.75} S \quad \text{(eq. 6)}$$

Where S is the two-phase suppression factor given as a function of the two-phase Reynolds number given as:

$$S = \left(1 + 2.56e^{-6} Re_{tp}^{1.17}\right)^{-1} \quad \text{(eq. 7)}$$

The two-phase Reynolds number is a function of liquid Reynolds number and Martinelli parameter function as:

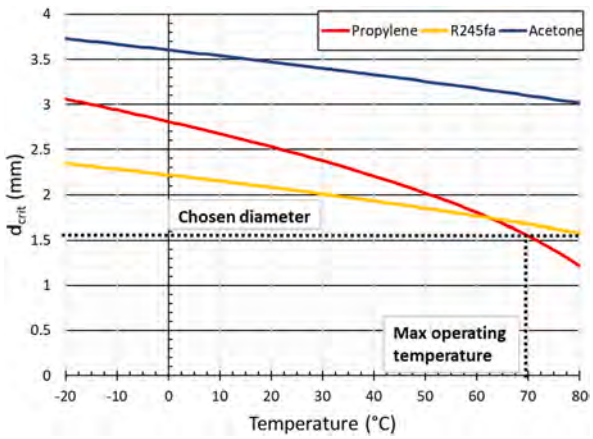

Fig. 2. Critical diameter of the chosen working fluids.

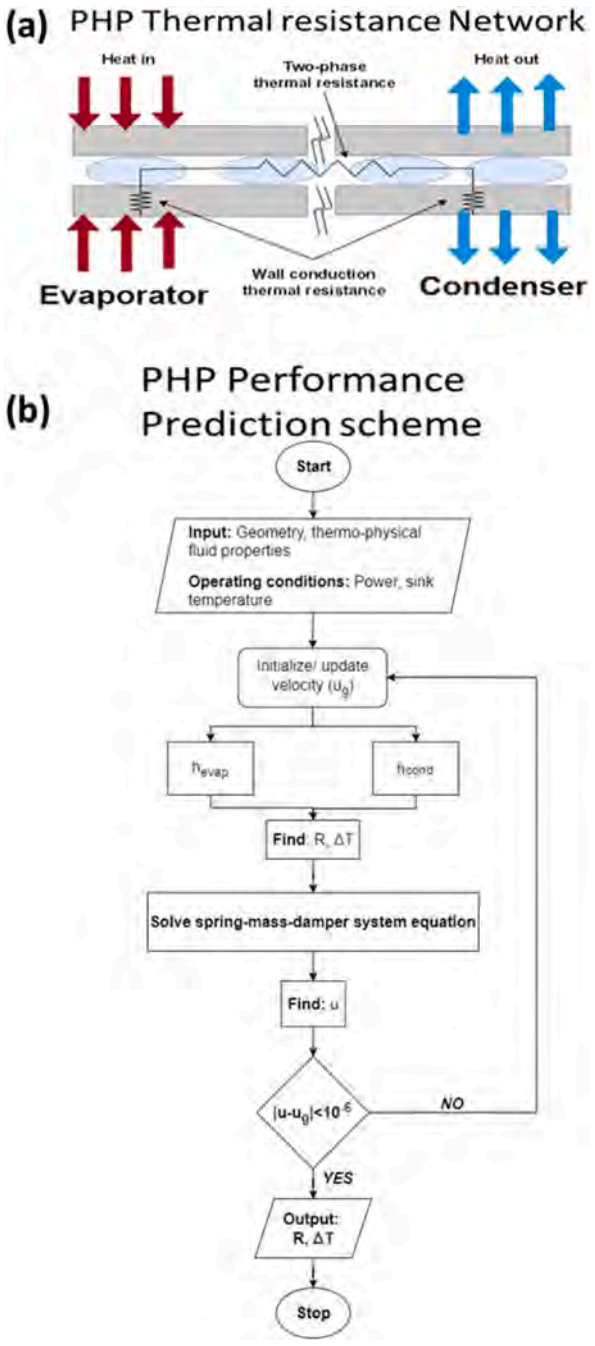

Fig. 3. (a) Schematic of PHP thermal resistance network; (b) Solution scheme for PHP performance prediction.

$$Re_{tp} = Re_l F(X_{tt})^{1.25} \quad \text{(eq. 8)}$$

The Martinelli function parameter takes the form:

$$F(X_{tt}) = \begin{cases} 1, X_{tt}^{-1} \le 0.1 \\ 2.35\left(0.213 + \frac{1}{X_{tt}}\right)^{0.736}, X_{tt}^{-1} > 0.1 \end{cases} \quad \text{(eq. 9)}$$

Where X_{tt} is the Martinelli parameter given as:

$$X_{tt} = \left(\frac{1-x}{x}\right)^{0.9} \left(\frac{\rho_v}{\rho_l}\right)^{0.5} \left(\frac{\mu_l}{\mu_v}\right)^{0.1} \quad \text{(eq. 10)}$$

Using the Martinelli function, the macroscopic convective heat transfer coefficient is given as:

$$h_{mac} = F(X_{tt}) h_l \quad \text{(eq. 11)}$$

Where h_l is the convective liquid heat transfer coefficient calculated according to the Dittus-Boelter correlation.

2.5.2. Condenser heat transfer

The two-phase condensation heat transfer coefficient can be calculated according to Shah correlation [30]:

$$h_{cond} = h_l \left((1-x)^{0.8} + \frac{3.8 x^{0.76} (1-x)^{0.04}}{\left(\frac{P}{P_{cr}}\right)^{0.38}} \right) \quad \text{(eq. 12)}$$

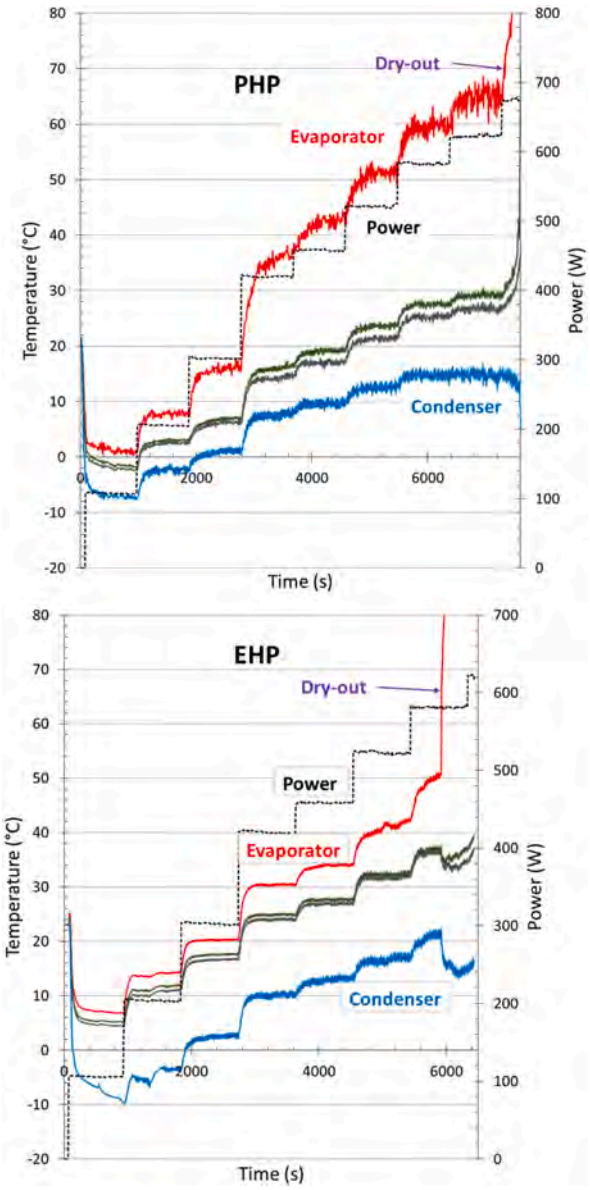

Fig. 4. Wall temperature profile of (a) PHP and (b) EHP heat spreaders.

2.5.3. Fluid pulsation in the PHP channels

The summation of interfacial, viscous damping, gravity, and vapor restoring forces acting on the liquid result in the equation of motion as [26]:

$$m\ddot{y} = A\left(\Delta P_g - \Delta P_v + \Delta P_\tau + \Delta P_K\right) \quad \text{(eq. 13)}$$

Accounting for bulk movement and rearranging above to represent a spring-mass-damper system gives:

$$m\ddot{y} + c\dot{y} + ky = b \quad \text{(eq. 14)}$$

Where the term on the right-hand side is the driving force arising from overall pressure drop due to evaporator and condenser temperature and is given as:

$$b = \frac{A\rho_v h_{fg}}{T_e}(\Delta T) \quad \text{(eq. 15)}$$

The spring restoring force coefficient (k) and damping coefficient (c) are given as:

$$k = \frac{A\rho_v RT}{L_v} \quad \text{(eq. 16)}$$

$$c = A\sum_{i=l,v}\left(f_i Re_i \frac{(\mu_i L_i)}{2d_h^2}\right) + A\Delta P_K \quad \text{(eq. 17)}$$

The first term on the right side corresponds to the viscous damping and the second term on the right-hand side corresponds to the pressure losses due to bends. Accounting for the bend length and the angle, the pressure loss in the bend can be calculated as:

$$\Delta P_{K,l} = \frac{1}{2} f_l \frac{\rho_l u^2}{2}\frac{\pi r_b}{d_h} + \frac{1}{2}k_b \rho_l u^2 \quad \text{(eq. 18)}$$

The above equation corresponds to single-phase liquid flow. Accounting for two-phase flow, the pressure drop due to bends is given as [32]:

$$\frac{\Delta P_K}{\Delta P_{K,l}} = 1 + \left(\frac{\rho_l}{\rho_v} - 1\right)\left(\left(1 + \frac{2.2}{k_b\left(2 + \frac{r_b}{d_h}\right)}\right)x(1-x) + x^2\right) \quad \text{(eq. 19)}$$

3. Results

The thermal performance of the heat spreaders was tested at a constant sink temperature of 40 °C. PHP was charged with the chosen fluids at up to 50% of the available volume. In the quasi-steady state testing, at a certain heater power, wall temperatures were recorded until a steady state. Then the heater power was increased. The cut-off condition was selected as either 150 °C maximum allowable heater temperature or dry-out of the heat spreader.

3.1. Thermal performance of EHP and PHP heat spreader with heat sink at −10 °C

The heat spreaders were tested with the cold plate at −10 °C. Only propylene-charged PHP was deemed suitable in this case based on its properties. For brevity, the temperature profile of the PHP and the EHP heat spreaders are shown only for this case in Fig. 4. The heat spreader condenser temperature increased with increasing heater power based on the condenser-sink heat transfer coefficient.

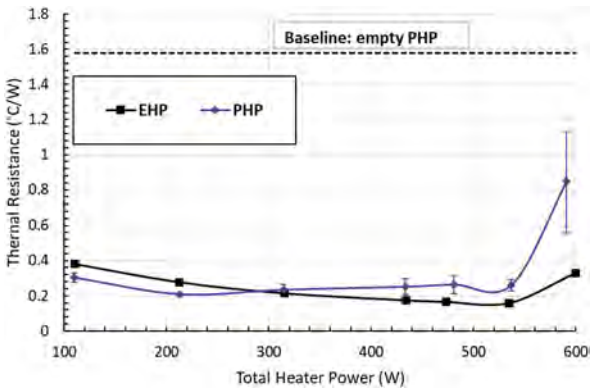

Fig. 5. Thermal performance of EHP and PHP heat spreaders.

With increasing heater power, the wall surface temperature increased for both PHP and the EHP heat spreader. The oscillation frequency in the PHP wall temperatures was found to be more pronounced at higher temperatures and heater power indicating good heat transfer characteristics due to pulsation of the working fluid. At around 600 W, the evaporator wall temperature drastically increased, while, at the same time, the condenser wall temperature decreased for both PHP and the EHP heat spreaders, indicating dry-out condition.

Fig. 5 shows the thermal resistance curves of the EHP and the PHP heat spreaders. The thermal resistance of the empty PHP is represented by the dashed line. From the calculation, the thermal conductivity of the empty PHP (baseline) was found to be 188 W/m-K. Until the heater power of 300 W, the thermal resistance of the PHP was lower than the EHP heat spreader. The PHP heat spreader thermal resistance was 0.21 °C/W at 200 W. Above 300 W, the thermal resistance of EHP was lower than the PHP. PHP showed dry-out characteristics as the heat spreader temperature increased, while the temperature was ideal for two-phase heat transfer with water in the EHP. Thermal resistance decreases with increasing heater power as the EHPs become more effective at a higher temperature. The thermal resistance of the EHP heat spreader was 0.16 °C/W at 535 W, at which point, the thermal resistance of the PHP was 0.26 °C/W.

3.2. *Thermal performance of the EHP and the PHP heat spreaders at other operating conditions*

The thermal performance characterization of the EHP and the PHP heat spreaders was performed with heat sink at 40 °C and 70 °C, respectively. The PHP was tested with all three working fluids: propylene, acetone, and R245fa up to 50% of the channel volume.

Fig. 6 shows the thermal resistance of the two heat spreaders with sink at 40 °C and 70 °C. In the 40 °C case, at lower heater powers of 20 W and 35 W, propylene PHP showed thermal resistance lower than 0.2 °C/W, but the thermal resistance increased above 35 W. The wall temperature profile showed aggressive oscillation behavior. On the other hand, the thermal performance of R245fa and acetone PHP improved with increasing heater power. This meant that R245fa and acetone were suitable for higher temperatures. The thermal resistance reduced drastically from above 1 °C/W at low heater power to 0.6 °C/W in the case of R245fa PHP and to 0.4 °C/W in the case of acetone PHP at around 200 W. The thermal resistance was further reduced to 0.57 °C/W with R245fa PHP and to 0.33 °C/W with acetone PHP at 300 W heater power. EHP heat spreader on the other hand showed almost constant thermal resistance at around 0.08 °C/W. For comparison, the conduction only heat spreader thermal resistance is shown as dashed lines, whose thermal resistance is 1.55 °C/W. In the case of 70 °C testing, Propylene PHP had low thermal resistance of 0.18 °C/W at lower heater power of 40 W, but the thermal resistance increased above this value indicating dry-out. R245fa PHP, on the other hand, did not operate. It must be noted that

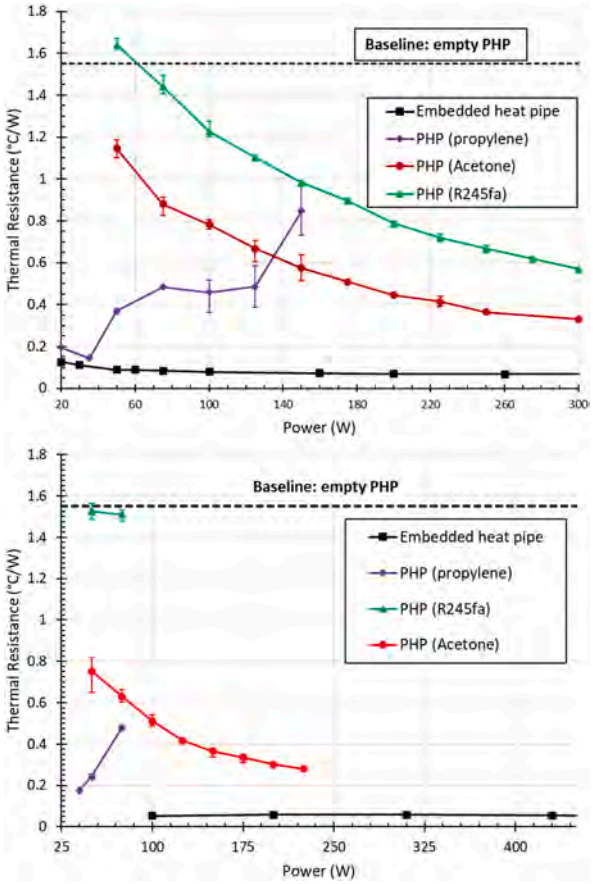

Fig. 6. Thermal performance curves of heat spreaders at (a) 40 °C and (b) 70 °C.

the Bond number limit of both PHP with propylene and R245fa is ~70 °C operating temperature, so they might not be suitable fluids. Performance of acetone PHP improved with thermal resistance decreasing from ~0.75 °C/W at 50 W to 0.28 °C/W at 225 W. The thermal resistance of the EHP almost stayed constant with varying heater power, indicating optimal performance.

From the present analysis, it was identified that propylene PHP was better than or similar to EHP at −10 °C sink temperature. At higher operating temperatures, the EHP performed better than propylene PHP. Although R245fa is a widely used two-phase fluid, acetone PHP performed well compared to R245fa PHP at 40 °C nominal operating temperature and 70 °C higher operating temperature.

3.3. Thermal conductivity of PHP and EHP heat spreaders

The thermal conductivity of the heat spreaders was calculated using Eq. (2). Fig. 7 shows the effective thermal conductivity of the PHP heat spreader charged with propylene (purple-unfilled), R245fa (green-gradient fill), and acetone (blue-solid) from the experiments performed. The thermal conductivity of the control (empty PHP) is shown as dashed black lines. At low heater powers below the PHP startup, the thermal conductivity can be lower than the control, because of additional fluid thermal resistance in the channels. However, after the startup, the thermal conductivity increases due to the two-phase operation of the working fluid. The highest thermal conductivity of 1400 W/m-K was achieved with propylene at 40 °C sink temperature at 2.7 W/cm^2 heater power. From thermal performance data, it was observed that the effective thermal conductivity gradually increased with a flattening trend for R245fa and acetone PHPs up to 34–38 W/cm^2 heat flux. In the case of propylene PHP at −10 °C, the effective thermal conductivity was typically between 700 and 1000 W/m-K. The thermal conductivity of EHPs was mostly greater than 1000 W/m-K.

The improvement in PHP and the EHP effective thermal conductivity over the aluminum conduction plate at their best operating conditions is shown in Table 1. The propylene PHP can yield effective thermal conductivity up to 7.8 times more than that of the conventional conduction-only plate, while R245fa PHP and acetone PHP can have up to 2.8 times (40 °C sink temperature) and 4 times (70 °C sink temperature) thermal conductivity improvement. EHP shows up to 7 times improvement over the conduction plate at −10 °C which increases up to 17.3 times at 70 °C sink temperature.

3.4. Performance comparison of numerical code against experimental data

The numerical model developed was validated against experimental data presented here and from the literature and is shown below in Fig. 8. Table 2 shows the vital geometric and operating conditions of the PHP test data from published literature. The last column shows the maximum variation in the performance data between the experimental data and the numerical data. The overall maximum deviation was found to be <33%, which is considered to be provide good validity of the developed mathematic model [33, 34].

Fig. 8 shows the performance comparison of the PHP model with the experimental data. For brevity, only a subset of experimental data for different working fluids and different operating conditions is presented here. The dashed line represents the thermal resistance trend predicted from the PHP model and the solid lines with markers are the experimental data. PHP performance data for propylene at −10 °C sink temperature and acetone at 40 °C are shown, along with other published data from the literature. For acetone, some deviation in predicted thermal resistance was observed at lower powers-near start-up conditions and errors associated with correlations at small operating powers and low temperatures. With increasing heater power, good agreement between the experimental data and the model was obtained. Likewise, good performance agreement with published experimental data found in the literature was found with the developed PHP thermal performance model. The experimental data used for validation in the above figure represents diverse data sets with various working fluids, operating conditions, and PHP geometries.

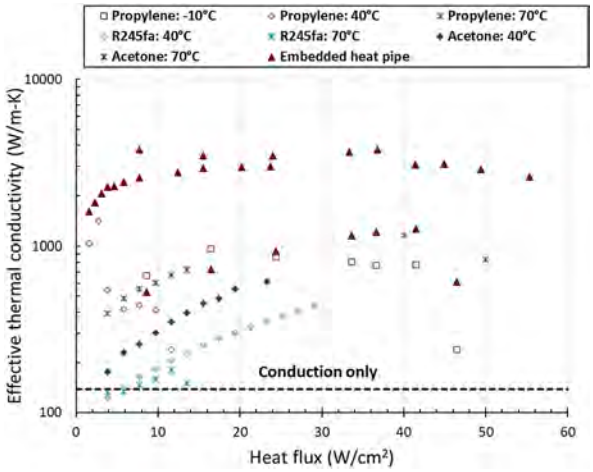

Fig. 7. Effective thermal conductivity of PHP vs Heat flux.

Table 1
Comparative highest effective thermal conductivity of the heat spreaders at their best operating performance.

Property	Propylene PHP	R245fa PHP	Acetone PHP	EHP
Temperature	−10 °C, 40 °C, 70 °C	40 °C	40 °C, 70 °C	−10 °C, 40 °C, 70 °C
Effective thermal conductivity (W/m-K)	969.8, 1407.2, 1149.8	444.7	612.5, 723.4	1267.1, 2998.6, 3107.4
Thermal conductivity improvement over conduction plate	5.4X – 7.8X	2.5X	3.2X – 4X	7X – 17.3X

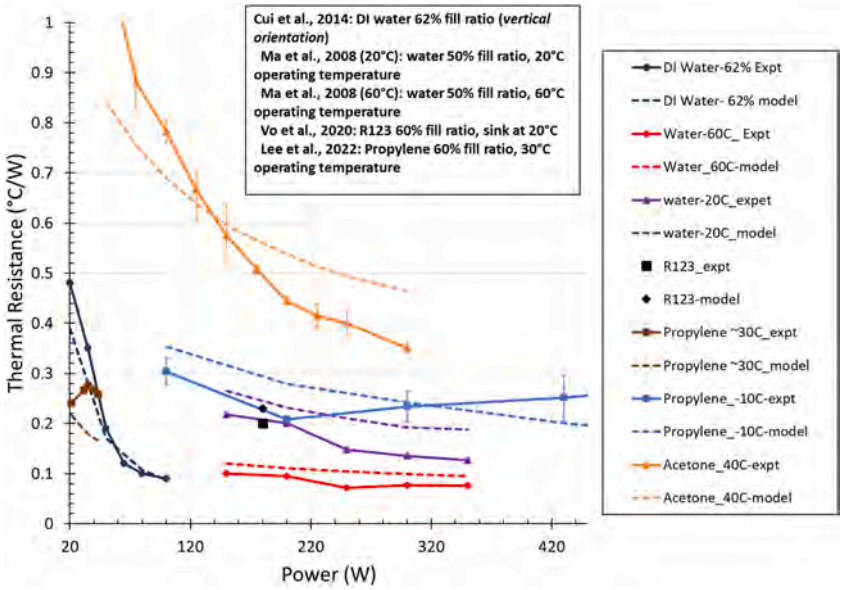

Fig. 8. Comparison of thermal resistance predicted by the PHP model and experimental data.

Table 2
Geometric information and operating conditions of the PHP from published literature used for model validation. The last column corresponds to the deviation in thermal performance prediction against experimentally noted thermal performance.

Reference	Working fluid	Operating temperature range (°C)/Heater Power (W)	Channel Diameter (mm)	Fill ratio (%)	Length of the evaporator (mm)/condenser (mm)/no of turns	Deviation in thermal performance $(\left\|\frac{R_{model}-R_{expt}}{R_{expt}}\right\| * 100)$ (%)
Cui et al. [35],	Deionized Water	20–90 °C	2	62	80/80/5	17.3
Lee et al. [36];	Propylene	30–40 °C	1.6	60	16.3/12.7/24	14.05
Ma et al. [37],	Water	20 °C	1.65	50	38/60/8	31.5
Ma et al. [37],	Water	60 °C	1.65	50	38/60/8	27.4
Vo et al. [38],	R123	180 W	1.85	60	130/135/8	15

4. Discussion of working fluid selection for PHP performance optimization

From the experiments, it was observed that the performance of (propylene) PHP was slightly better than or similar to that of EHPs at low temperatures and low power for moderate temperatures. The performance of R245fa and acetone PHP improved with increasing heater power but was lower than EHPs. The performance of PHP, in general, was better than the aluminum conduction plate.

For a chosen PHP geometry, within the operating limits, it is surmised that the working fluid selection is an important criterion in optimizing the PHP performance. Fig. 9 shows the saturation pressure curves and the merit number [39] of several applicable PHP working fluids. The merit number curves shown are based on the thermal performance and based on the heat transfer limits. Water is not shown here due to its incompatibility with aluminum. Propylene has a high saturation pressure and merit number, on par with ammonia and slightly greater than R134a. Possibly, the high merit number must have resulted in high-performing PHP at low temperatures. Also, the global warming potential (GWP) of propylene is only 2. The GWP of ammonia is slightly higher at 3.1 but for R134a is 1430. A potential trade-off in favor of ammonia then is the larger critical diameter (>3 mm) in comparison to propylene (1.6 mm). From the model and the literature [23], it is noted that a larger channel diameter improves PHP performance. If a larger diameter is

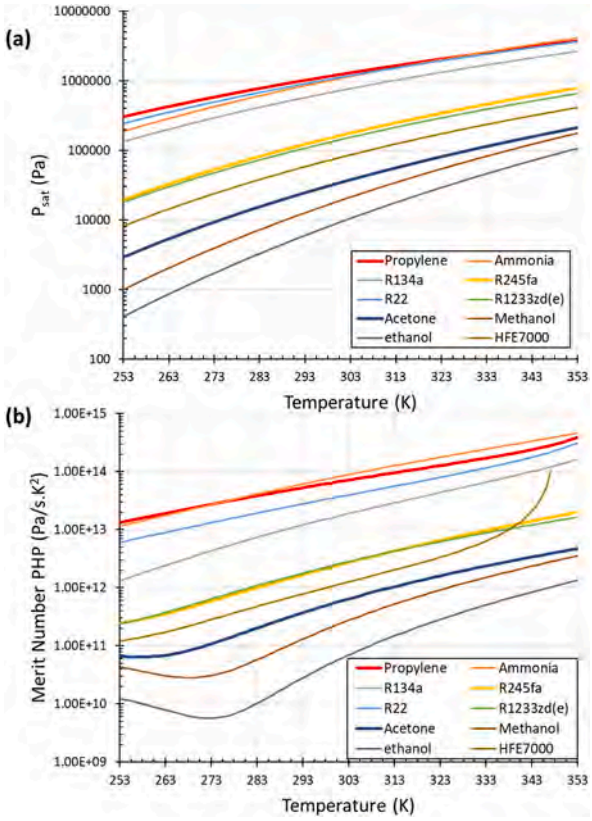

Fig. 9. (a) Saturation pressure curves and (b) Merit number of applicable PHP working fluids.

considered, ammonia-charged PHP thus can be better performing than propylene PHP. R134a charged PHP is inconsistent in operation [40]. These three fluids are also flammable, so charging them requires stringent safety protocols. These fluids are suitable only up to 70 °C considering diminishing heat transfer limits [19,41], very high vapor pressures, and PHP wall thickness requirements [18,27]. For moderate (e.g., >40 °C) to high-temperature applications, R245fa has better properties than acetone. However, from experiments and Fig. 2, it was determined that the performance of R245fa-charged PHP was lower than acetone partly due to channel limitations. From the literature, it was determined that for applications up to 90 °C –HFO-1234yf [42] and for moderate to high-temperature applications 150 °C– HFO-1336mzz(z) [43] could potentially make PHP competitive with EHPs. These also have low global warming potential.

The mass of PHP and EHP for the chosen heat spreader plate dimensions is shown in Table 3. Note that, the EHP seems heavier but in real applications, some redundant structure material of the heat spreader can be further removed so the overall mass will be similar to a PHP-based spreader and aluminum plate. In additively manufactured PHPs, capillary channels can easily accommodate sharp turns and corners [36,44] which is usually avoided in the case of EHP due to the rigid heat pipe envelope.

5. Conclusion and recommendation

The thermal performance of pulsating heat pipe (PHP) and EHP heat spreaders was determined and compared experimentally at various sink temperatures for potential low to medium-temperature applications. PHP was charged with propylene, R245fa, and acetone up to 50% of the volume. EHPs consisted of 8 Cu–H_2O heat pipes. At low temperatures, the performance of propylene PHP was better than or similar to EHPs, with up to 7.8 times higher effective thermal conductivity over conventional aluminum conduction plates. The effective thermal conductivity of EHPs was up to 7 times higher than the conventional conduction plate. At moderate temperatures >40 °C, propylene PHP dries out at heater power below 150 W. Both R245fa and acetone-charged PHP show improvement in performance with increasing heater power. Under the test conditions, up to 2.8 times improvement in thermal conductivity over conventional plate can be obtained with R245fa PHP, while the effective thermal conductivity can be up to 4 times more with acetone PHP. The EHP performs significantly better than the PHP at temperatures higher than 40 °C because heat transfer in EHPs is by the latent heat of vapor, while, on the other hand, PHPs have a significant contribution from the sensible heat of the working fluid. Effective thermal conductivity improvement of up to 17.3 times can be obtained with EHPs over a conduction plate. At a lower sink temperature of −10 °C, the thermal performance of propylene PHP is slightly better than the EHP but mostly comparable. PHP has the potential to perform better than EHP but the performance depends on several parameters like geometry, working fluid, operating temperature etc. As such, more work must be focused to determine the appropriate heat spreader for a given application. EHP is a

Table 3
Mass comparison of PHP and EHP heat spreaders.

Parameter	Propylene PHP	R245fa PHP	Acetone PHP	Embedded Cu–H_2O heat pipe	Aluminum plate (g)
Mass (g)	335.82	344.90	338.65	373.42	353.32
Change in mass (%)	−4.95%	−2.38%	−4.15%	+5.69%	–

mature technology [45], so recommendations on improving the knowledge on PHP heat spreaders are mentioned below.

- In the context of low-temperature application, propylene PHP showed comparable or better performance than EHP. But the PHP operated in partial dry-out mode in comparison to EHP at higher temperature. The shift in behavior from normal operation to partial and/or full dry-out mode must be identified for a given PHP either experimentally or mathematically.
- In the case of medium temperature range applications, low GWP fluids like HFO1234yz/HFO1336mzz were identified to have high PHP merit number. Comprehensive PHP testing must be performed to experimentally determine suitable PHP working fluid for a given temperature range that can compare against EHP.
- It was identified that shape conformal PHPs can be fabricated making it versatile for various electronics devices requiring complex heat spreading geometry. Usually, additive manufacturing (AM) is employed as the standard fabrication method. In light of employing AM techniques, it is important to recognize the performance of conventionally diffusion bonded PHP against AM-PHP. Additionally, the improvement in AM-PHP start-up due to relatively rough channel finish can provide important insight into the influence of fabrication technique on PHP performance.
- Along with fluid selection, it is imperative to have optimal fluid ratio. While, literature focused on fluid charge ratio in terms of PHP performance, from their trends, it can be inferred that fluid charge ratio is directly proportional to dry-out limit and also influences start-up.
- Along with fluid selection, future works must emphasize on the performance of PHP and EHP heat spreaders for various evaporator-condenser configurations and sizes including heater (evaporator) length, condenser length, distance between the evaporator-condenser length, shape of the fluid channels, etc.

As research into PHP heat spreaders improve, it can be summarized that they are good alternative to existing (or already mature) EHP solutions thereby, the final user has the choice depending on the mass sensitivity, shape matching, and cost requirements.

CRediT authorship contribution statement

Sai Kiran Hota: Conceptualization, Methodology, Software, Validation, Investigation, Writing – original draft. **Kuan-Lin Lee:** Conceptualization, Methodology, Writing – review & editing, Supervision, Funding acquisition. **Brett Leitherer:** Methodology, Investigation. **George Elias:** Methodology, Software, Investigation. **Greg Hoeschele:** Methodology, Resources. **Srujan Rokkam:** Writing – review & editing, Supervision, Funding acquisition.

Declaration of competing interest

The authors declare that they have no known competing financial interests or personal relationships that could have appeared to influence the work reported in this paper.

Data availability

Data will be made available on request.

Acknowledgements

This work was partially funded by the IR&D program of Advanced Cooling Technologies, Inc. and the NASA SBIR Phase II program (#80NSSC22CA205). We would like to acknowledge support from Dr. Jeffrey Diddion and Dr. Sergey Semonev. In addition, we would like to acknowledge Dr. Richard Bonner, former ACT-R&D Vice President for his technical inputs during the development of the manuscript. We would like to appreciate the contributions of R&D technicians, including Phil Texter, Justin Boyer, Eugene Sweigart, and Jonathan Murray, as well as the support from the PD and OPS teams of ACT.

References

[1] H.M. Tong, Y.S. Lai, C.P. Wong, Advanced Flip Chip Packaging, Springer, New York, 2013.
[2] S.M.S. Murshed, C.A.N. De Castro, A critical review of traditional and emerging techniques and fluids for electronics cooling, Renew. Sustain. Energy Rev. 78 (2017) 821–833.
[3] A. Slippey, W. Anderson, M. Ellis, C. Hose, J. Schmidt, J. Weyant, Thermal Management Technologies for Embedded Cooling Applications," 17th IEEE Intersociety Conference on Thermal and Thermochemical Phenomena in Electronic Systems, 2018, pp. 556–561.
[4] J. Weyant, S. Garner, M. Johnson, M. Occhionero, Heat Pipe Embedded AlSiC Plates for High Conductivity - Low CTE Heat Spreaders," 12th IEEE Intersociety Conference on Thermal and Thermomechanical Phenomena in Electronic Systems, IEEE, 2010.
[5] K. Zhu, M. Zheng, B. Wang, B. Dai, Y. Wang, J. Wei, X. Chen, Experimental Study of Energy Saving Performances in Chip Coolant by Using Heat Sink with Embedded Heat Pipe," the 8th International Conference on Applied Energy, ICAE, 2016.

[6] T.M. Salem, F.S. Khosroshahi, M. Arik, M.O. Hamdan, M. Budakli, Numerical and experimental analysis of a heat-pipe-embedded printed circuit board for solid state lighting applications, Exp. Heat Tran. 32 (1) (2019) 1–13.
[7] M. Muneeshwaran, Y.J. Lee, C.C. Wang, Performance improvement of heat sink with vapor chamber base and heat pipe, Appl. Therm. Eng. 215 (2022), 118932.
[8] M.T. Ababneh, C. Tarau, W.G. Anderson, A.R.A. Hernandez, S. Ortega, J.T. Farmer, R. Hawkins, Demonstration of copper-water heat pipes embedded in high conductivity (HiK(TM)) plates in the advanced Space thermal eXperiment (APTx) on the international Space station, in: 48th International Conference on Environmental Systems, 2018. Albuquerque, NM, USA.
[9] M. Marengo, V. Nikolayev, Chapter 1. Pulsating heat pipes: experimental analysis, design and applications, in: Encyclopedia of Two-phase Heat Transfer and Flow IV: Modeling Methodologies, Boiling of CO2, and Micro-two Phase Cooling Volume 1: Modeling of Two-phase Flows and Heat Transfer, 2018, pp. 1–62.
[10] S.K. Hota, K.-L. Lee, G. Hoeschele, T. Mcfarland, S. Rokkam, R.W. Bonner, Experimental comparison of two-phase heat spreaders for Space modular electronics, in: 52nd International Conference on Environmental Systems (Accepted for Presentation), 2023. Calgary, Canada.
[11] M. Winkler, D. Rapp, A. Mahlke, F. Zunftmeister, M. Vergez, Wischerhoff, O. Schäfer-Welson, Small-sized pulsating heat pipes/oscillating heat pipes with low thermal resistance and heat transport capability, Energies 13 (7) (2020) 1736.
[12] S.K. Hota, K.-L. Lee, G.B.R.R.S. Hoeschele, Experimental comparison on thermal performance of pulsating heat pipe and embedded heat pipe heat spreaders, in: 39th Annual Semiconductor Thermal Measurement, Modeling and Management Symposium, 2023. San Jose, CA, USA.
[13] M.P. Hoesing, G.J. Michna, Integration of a pulsating heat pipe in a Flat Plate heat sink, in: Proceedings of the ASME 2014 12th International Conference on Nanochannels, Microchannels, and Minichannels, Chicago, IL, USA, 2014.
[14] F.F. Luan, H. Lu, H.B. Ma, An experimental investigation of an oscillating heat pipe heat spreader, J. Therm. Sci. Eng. Appl. 7 (2015), 021005.
[15] W. Qu, B. Yang, Performances of Flat Plate pulsating heat pipes, in: 2nd Micro/Nano Heat and Mass Transfer International Conference, 2009. Shanghai, China.
[16] S.M. Thompson, Z.S. Aspin, N. Shamsaei, A. Elwany, L. Bian, Additive Manufacturing of heat exchangers: a case study on a multi-layered Ti-6Al-4U Oscillating Heat Pipe, Addit. Manuf. 163–174 (2015) 8.
[17] B. Tian, D. Yang, H. Ma, J. Xu, D. Liang, A manufacturing method of integrated ceramic heat spreaders embedded with interconnected microchannels, Mater. Des. 180 (2019), 107969.
[18] S.K. Hota, K.-L. Lee, G. Hoeschele, R.W. Bonner, S. Rokkam, Performance investigation on different form factor embedded heat pipe and pulsating heat pipe heat spreaders, in: Proceedings of the 17th International Heat Transfer Conference, IHTC-17 (accepted for presentation), Cape Town, South Africa, 2023.
[19] B. Drolen, C. Smoot, Performance limits of oscillating heat pipes: theory and validation, J. Thermophys. Heat Tran. 31 (4) (2017) 920–936.
[20] W. Qu, H.B. Ma, Theoretical analysis of startup of a pulsating heat pipe, Int. J. Heat Mass Tran. 50 (2007) 2309–2316.
[21] V.M. Patel, M.H.B. Gaurav, Influence of working fluids on startup mechanism and thermal performance of a closed loop pulsating heat pipe, Appl. Therm. Eng. 110 (2017) 1568–1577.
[22] M. Nazari, M. Ahmadi, R. Ghasempour, M. Shafii, How to improve the thermal performance of pulsating heat pipes: a review on working fluid, Renew. Sustain. Energy Rev. 91 (2018) 630–638.
[23] V. Ayel, M. Slobodeniuk, R. Bertossi, C. Romestant, Y. Bertin, Flat plate pulsating heat pipes: a review on the thermohydraulic principles, thermal performances and open issues, Appl. Therm. Eng. 197 (2021), 117200.
[24] Y. Zhang, A. Faghri, Advances and unsolved issues in pulsating heat pipes, Heat Tran. Eng. 29 (2008) 20–44.
[25] G. Gürsel, A.J.H. Frijns, F.G.A. Homburg, A.A. van Steenhoven, A mass-spring-damper model of a pulsating heat pipe with a non-uniform and asymmetric filling, Appl. Therm. Eng. 91 (2015) 80–90.
[26] M. Mameli, M. Marengo, S. Zinna, Numerical model of a multi-turn closed loop pulsating heat pipe: effects of the local pressure losses due to meanderings, Int. J. Heat Mass Tran. 55 (2012) 1036–1047.
[27] ANSI/VITA, Mechanical Standard for VPX REDI Conduction Cooling, VPX, 2020.
[28] B. Guenin, Packaging challenges for high heat flux devices, Electron. Cooling 12 (3) (2006) 28.
[29] J.C. Chen, Correlation for boiling heat transfer to saturated fluids in convective flow, Ind. Eng. Chem. Process Des. Dev. 5 (3) (1966) 322–329.
[30] M.M. Shah, A general correlation for heat transfer during film condensation inside pipes, Int. J. Heat Mass Tran. 22 (4) (1979) 547–556.
[31] H. Ma, Oscillating Heat Pipes, Springer, New York, 2015.
[32] D. Chisholm, Two-phase flow in bends, Int. J. Multiphas. Flow 6 (4) (1980) 363–367.
[33] S.K. Hota, V. Duong, G. Diaz, Two-phase flow performance prediction for minichannel solar collectors, Heat Mass Tran. 56 (2020) 109–120.
[34] F.P. Incropera, D.P. Dewit, T.L. Bergman, A.S. Lavine, Fundamentals of Heat and Mass Transfer, sixth ed., John Wiley & Sons, 2006.
[35] X. Cui, Y. Zhu, Z. Li, S. S, Combination study of operation characteristics and heat transfer mechanism for pulsating heat pipe, Appl. Therm. Eng. 65 (2014) 394–402.
[36] K.L. Lee, S.K. Hota, A. Lutz, S. Rokkam, Advanced two-phase cooling system for modular power electronics, in: 51st International Conference on Envrionmental Systems, 2022. St. Paul, MN.
[37] H.B. Ma, B. Borgmeyer, P. Cheng, Y. Zhang, Heat transport capability in an oscillating heat pipe, J. Heat Tran. 130 (8) (2008), 081501.
[38] D.T. Vo, H.T. Kim, J. Ko, K.H. Bang, An experiment and three-dimensional numerical simulation of pulsating heat pipes, Int. J. Heat Mass Tran. 150 (2020), 119317.
[39] J. Kim, S.J. Kim, Experimental investigation on working fluid selection in a micro pulsating heat pipe, Energy Convers. Manag. 205 (2020), 112462.
[40] K.A. Stevens, S.M. Smith, B.S. Taft, Variation in oscillating heat pipe performance, Appl. Therm. Eng. 149 (2019) 987–995.
[41] R. Wilcoxon, J. Boswell, B. Drolen, Oscillating heat pipe thermal performance and stability limits, in: 38th SEMI-THERM Symposium, 2022.
[42] B.S. Taft, A.D. Williams, B.L. Drolen, Working fluid selection for pulsating heat pipes, in: 42nd AIAA Thermophysics Conference, 2011. Honolulu, Hawaii.
[43] K. Kontomaris, HFO-1336mzz-z: high temperature chemical stability and use as a working fluid in organic rankine cycles, in: 15th International Refrigeration and Air Conditioning Conference, 2014. Purdue.
[44] H. Tang, Y. Tang, Z. Wan, J. Li, W. Yuan, L. Lu, Y. Li, K. Tang, Review of applications and developments of ultra thin micro heat pipes for electronic cooling, Appl. Energy 223 (2018) 383–400.
[45] [Online]. Available: https://www.1-act.com/resources/heat-pipe-calculator/.